Articles in PresS. J Neurophysiol (October 2, 2013). doi:10.1152/jn.01046.2012

Innovative Methodology (J Neurophysiol) – Revision 1

Bayesian Decoding using Unsorted Spikes in the Rat Hippocampus

Fabian Kloosterman[1,2,3,4,5], **Stuart P. Layton**[1,2], **Zhe Chen**[1,2,6] and **Matthew A. Wilson**[1,2]

[1]*Department of Brain and Cognitive Sciences, Massachusetts Institute of Technology, Cambridge, Massachusetts;* [2]*Picower Institute for Learning and Memory, Massachusetts Institute of Technology, Cambridge, Massachusetts;* [3]*NERF, Leuven, Belgium;* [4]*imec, Leuven,* [5]*Laboratory of Biological Psychology, Department of Psychology, KU Leuven, Leuven, Belgium; and* [6]*Neuroscience Statistics Research Lab, Massachusetts General Hospital, Harvard Medical School, Boston, Massachusetts*

Running Head: Bayesian decoding using unsorted spikes

Correspondence: Fabian Kloosterman, NERF/imec, Kapeldreef 75, B-3001 Leuven. Belgium
E-mail: fabian.kloosterman@nerf.be
Phone: +003216283514

Figures: 5

Tables: 4

Copyright © 2013 by the American Physiological Society.

Abstract

A fundamental task in neuroscience is to understand how neural ensembles represent information. Population decoding is a useful tool to extract information from neuronal populations based on the ensemble spiking activity. We propose a novel Bayesian decoding paradigm to decode unsorted spikes in the rat hippocampus. Our approach uses a direct mapping between spike waveform features and covariates of interest, and avoids accumulation of spike-sorting errors. Our decoding paradigm is nonparametric, encoding model-free for representing stimuli, and extracts information from all available spikes and their waveform features. We apply the proposed Bayesian decoding algorithm to a position reconstruction task for freely behaving rats based on tetrode recordings of rat hippocampal neuronal activity. Our detailed decoding analyses demonstrate that our approach is efficient and better utilizes the available information in the non-sortable hash than the standard sorting-based decoding algorithm. Our approach can be adapted to an online encoding/decoding framework for applications that require real time decoding, such as brain-machine interfaces.

Keywords: neural decoding, spatial-temporal Poisson process, population codes, kernel density estimation, spike sorting

INTRODUCTION

Features of sensory stimuli and intended motor actions are reflected in the activity of neuronal ensembles that are distributed across the brain (Sanger, 2003; Huys et al., 2007; Boloori et al., 2010). A fundamental goal in neuroscience is to understand how the information about external stimuli is transformed into neural activity patterns and how this information is represented in the brain. The relationship between stimuli and neural activity can be described by statistical encoding models (Brown et al., 1998; Sanger, 2003; Truccolo et al., 2005; Paninski et al., 2007). Inversion of these encoding models, i.e. extraction of information about the stimulus from observed neural activity ("neural decoding"), aids in revealing the principles of the encoding process (Quian Quiroga and Panzeri, 2009). Neural decoding can also be applied to uncover internal neural representations in the absence of an overt stimulus, for example the re-expression of spatial sequences in the hippocampus (Davidson et al., 2009; Gupta et al., 2010) or movement intentions in motor cortices (Georgopoulos et al., 1986; Zhuang et al., 2010). Decoding motor plans in particular is an important part of the development of neural prosthetics and brain-machine interfaces which may restore motor function in patients with neurological damage (Chapin, 2004; Schwartz et al., 2006; Hochberg et al., 2012).

The principal goal of neural decoding is to extract as much information about a stimulus as possible from a neural signal. As with all signal processing, any additional operation on the raw signal in neural decoding adds complexity and leads to possible loss of information. Most approaches for decoding neural spiking activity rely on the intermediate step of sorting spike waveforms into groups of single units. The spike sorting process is subject to at least two

problems that could affect decoding performance. The first issue is that the goal of neural decoding to minimize the decoding error is substantially different from the goal to label each spike uniquely and confidently with the identity of the cell that emitted it. In particular spike sorting is generally conservative and many spikes are left unclassified in an attempt to minimize classification errors. However, spikes thrown out during the sorting process could still convey information about the stimulus and hence contribute to decoding performance. Second, inherent to spike sorting are misclassification errors – that is, incorrect assignment of spikes to a unit. Theoretical analysis has shown that different spike sorting errors have various impacts on information capacity, with false positive errors having the most serious effect (Goodman and Johnson, 2008). Another potential source of misclassification is the use of hard decision boundaries – it has been suggested that a soft decision boundary is more appropriate for evaluating neural ensemble codes (Wood and Black, 2008).

To maximize the stimulus information extracted from neural spiking activity, we propose a novel Bayesian decoding paradigm that does not require the intermediate step of spike sorting. Key in our approach is a direct mapping between the raw data (i.e. spike waveform features) and the stimulus in a joint probability distribution. In contrast to previous work, our approach does not assume a parametric or biophysical model to describe the relation between stimulus and neural activity.

The performance of the new decoding approach is analyzed by applying it to hippocampal population recordings in order to estimate the location of a rat on a track.

METHODS

Spike feature decoding framework

ENCODING MODEL. The ultimate goal of our method is to reconstruct a sensory stimulus, motor action or other covariate (from here on referred to as "stimulus") from neuronal spiking activity recorded from an array of sensors (e.g. single wire electrodes, stereotrodes or tetrodes). First, we build an encoding model that relates the neural activity on a single sensor to the stimulus of interest. Let's assume that in the time period $(0, T]$ we recorded the time varying stimulus vector $\boldsymbol{x}(t)$ as well as N discrete spike events and their waveforms at times t_n, with $0 < t_1 < t_2 < \cdots < t_N \leq T$. For simplicity we assume that all spikes occur conditionally independent of previous spikes and treat the detected spikes as a spatio-temporal Poisson process, or equivalently as a marked temporal Poisson process, in which the spatial component (the "mark") is a vector space S of spike waveform features $\boldsymbol{a} \in S$. Examples of typical waveform features are peak amplitude, spike width, extracted principal components or other derived features. The same waveform features are generally used by spike sorting processes to extract single units from multi-unit activity. In our approach the spike sorting step is bypassed by creating a direct mapping between spike waveform features and stimulus (Fig. 1). The spatio-temporal Poisson process is fully characterized by its generalized rate function $\lambda(\boldsymbol{a}, t)$. In cases when the rate is determined by the stimulus of interest, the rate function can be re-expressed as $\lambda(\boldsymbol{a}, t) = \lambda(\boldsymbol{a}, \boldsymbol{x}(t))$. Here, $\lambda(\boldsymbol{a}, \boldsymbol{x})$ can be viewed as a tuning curve which relates the average rate of spike events with waveform features $\boldsymbol{a}$ to the stimulus $\boldsymbol{x}$.

To compute the probability that we observe n spikes with associated features $\boldsymbol{a}_{1:n}$ in a small time window $[t, t + \Delta t)$ in the presence of a known stimulus, the waveform feature space S is first

divided into J non-overlapping regions: $S \equiv (S_1 \cup S_2 \cup \cdots \cup S_J)$. Each region S_j contains n_j spikes, which is a subset of the observed n spikes (i.e. $\sum_{j=1}^{J} n_j = n$). The expected number of spikes in each region S_j follows a Poisson distribution with rate function: $\lambda_{S_j}(\boldsymbol{x}) = \int_{S_j} \lambda(\boldsymbol{a}, \boldsymbol{x}) d\boldsymbol{a}$. The likelihood of finding exactly $n_{1:J}$ spikes in regions $S_{1:J}$ can be computed from the product of Poisson likelihoods of all regions:

$$P(\boldsymbol{a}_{1:n}|\boldsymbol{x}) = P(n_{1:J}|\boldsymbol{x}) = \prod_{j=1}^{J} P(n_j|\boldsymbol{x}) = \prod_{j=1}^{J} Poisson\left(n_j; \lambda_{S_j}(\boldsymbol{x})\right)$$
$$= \frac{\left[\prod_{j=1}^{J} \left(\Delta t \int_{S_j} \lambda(\boldsymbol{a}, \boldsymbol{x}) d\boldsymbol{a}\right)^{n_j}\right]\left[e^{-\Delta t \sum_{j=1}^{J} \int_{S_j} \lambda(\boldsymbol{a}, \boldsymbol{x}) d\boldsymbol{a}}\right]}{\prod_{j=1}^{J} n_j!} \quad (1)$$

In the limiting case when regions $S_{1:J}$ become sufficiently small such that $n_{1:J}$ are equal to 0 or 1 within the time interval Δt, the likelihood can be rewritten as:

$$P(\boldsymbol{a}_{1:n}|\boldsymbol{x}) = (\Delta t)^n \left[\prod_{i=1}^{n} \lambda(\boldsymbol{a}_i, \boldsymbol{x})\right]\left[e^{-\Delta t \lambda(x)}\right] \quad (2)$$

This likelihood function, when calculated for all possible waveform feature vectors $\boldsymbol{a}$, completely characterizes the encoding process for a single sensor. For multiple sensors, assuming conditional spiking independence between sensors (i.e., each sensor records from an independent population of neurons), the joint data likelihood can be computed as a product of individual likelihoods contributed by each sensor. For K sensors and n_k spike events on the k-th electrode, the joint likelihood is given by:

$$P(\boldsymbol{a}^{1:K}|\boldsymbol{x}) = \prod_{k=1}^{K} P(\boldsymbol{a}_{1:n_k}|\boldsymbol{x}) \quad (3)$$

RELATION TO ENCODING WITH SPIKE SORTED UNITS OR MULTI-UNIT ACTIVITY. It is possible to

choose the spike feature $\boldsymbol{a}$ such that it is a discrete scalar variable that represents cell identity (for example obtained through a spike sorting procedure). In that case, each region S_j can be constructed such that it corresponds to a single cell c. This means that $\lambda_c(x) = \lambda_{S_j}(x)$ is the tuning curve of cell c and $n_c = n_j$ is the number of spikes emitted by cell c. By rewriting Eq. 1 we recover the likelihood for a population of spike sorted cells as a special case (Zhang et al., 1998):

$$P(n_{1:C}|\boldsymbol{x}) = \left[\frac{(\Delta t)^N}{\prod_{c=1}^{C} n_c!}\right]\left[\prod_{c=1}^{C} \lambda_c(\boldsymbol{x})^{n_c}\right]\left[e^{-\Delta t \sum_{c=1}^{C} \lambda_c(\boldsymbol{x})}\right] \tag{4}$$

where C is the total number of cells and $N = \sum_{c=1}^{C} n_c$ is the total number of spike events. When all spikes are considered part of a single multi-unit cluster and spike features $\boldsymbol{a}$ are ignored, then the likelihood can be further simplified to:

$$P(N|\boldsymbol{x}) = \left[\frac{(\Delta t)^N}{N!}\right]\lambda(\boldsymbol{x})^N\left[e^{-\Delta t \lambda(\boldsymbol{x})}\right] \tag{5}$$

EVALUATION OF THE LIKELIHOOD. To compute the likelihood in Eq. 2, representations of the generalized rate function $\lambda(\boldsymbol{a}, \boldsymbol{x})$ and its marginal rate function $\lambda(\boldsymbol{x})$ need to be constructed. A parametric model of the rate functions would allow for straightforward evaluation during decoding, however, it is not clear what model, if any, would be appropriate. In contrast, non-parametric models provide a more flexible estimate of the rate functions. Here we used kernel-density based estimators of the rate functions.

To construct the kernel-density estimators, the generalized rate function $\lambda(\boldsymbol{a}, \boldsymbol{x})$ and the marginal rate function $\lambda(\boldsymbol{x})$ are decomposed into spike event probability distributions ($p(\boldsymbol{a}, \boldsymbol{x})$ and $p(\boldsymbol{x})$) and a stimulus probability distribution ($\pi(\boldsymbol{x})$):

$$\lambda(\boldsymbol{a},\boldsymbol{x}) = \frac{spikecount(\boldsymbol{a},\boldsymbol{x})}{occupancy(\boldsymbol{x})} = \frac{N}{T}\frac{p(\boldsymbol{a},\boldsymbol{x})}{\pi(\boldsymbol{x})} = \mu\frac{p(\boldsymbol{a},\boldsymbol{x})}{\pi(\boldsymbol{x})} \tag{6}$$

$$\lambda(\boldsymbol{x}) = \mu\frac{p(\boldsymbol{x})}{\pi(\boldsymbol{x})} \tag{7}$$

148 Here, *spikecount* represents the number of spikes with features $\boldsymbol{a}$ that occurred at stimulus $\boldsymbol{x}$,
149 *occupancy* represents the total presentation time of stimulus $\boldsymbol{x}$; N is the total number of spikes
150 recorded in the time interval $(0, T]$ and μ is the average spiking rate.
151 The probability distributions $p(\boldsymbol{a},\boldsymbol{x})$, $p(\boldsymbol{x})$ and $\pi(\boldsymbol{x})$ can be estimated using the following
152 multivariate kernel density estimators:

$$p(\boldsymbol{a},\boldsymbol{x}) = \frac{1}{N}\sum_{n=1}^{N} K_{H_{ax}}\left(\begin{bmatrix}\boldsymbol{a}\\ \boldsymbol{x}\end{bmatrix} - \begin{bmatrix}\tilde{\boldsymbol{a}}_n\\ \tilde{\boldsymbol{x}}_n\end{bmatrix}\right) \tag{8}$$

$$p(\boldsymbol{x}) = \frac{1}{N}\sum_{n=1}^{N} K_{H_x}(\boldsymbol{x} - \tilde{\boldsymbol{x}}_n) \tag{9}$$

$$\pi(\boldsymbol{x}) = \frac{1}{R}\sum_{r=1}^{R} K_{H_x}(\boldsymbol{x} - \tilde{\boldsymbol{x}}_r) \tag{10}$$

153 Here, $\{\tilde{\boldsymbol{a}}_n, \tilde{\boldsymbol{x}}_n\}_{n=1}^{N}$ represents the set of N spikes with associated feature vectors and stimuli
154 which are collected during the encoding phase. $\{\tilde{\boldsymbol{x}}_r\}_{r=1}^{R}$ represents the set of R observed (or
155 chosen) stimuli, which are generally sampled at regular time intervals during the encoding stage.
156 $K_H(\cdot)$ is a kernel function with bandwidth matrix H. H_x represents the bandwidth matrix for the
157 stimulus only, and H_{ax} represents the combined bandwidth matrix for spike features and stimulus.
158 Examples of kernels that may be used are: Gaussian, Epanechnikov, uniform, von Mises (for
159 circular variables) or Kronecker delta (for discrete variables).
160 The bandwidth of a kernel determines the amount of smoothing that is applied to the underlying
161 data and therefore has a strong influence on the shape of the final density estimate. Determining
162 the optimal full multivariate bandwidth matrix H is computationally and mathematically

challenging. In practice, a simplified parameterization of the kernel is generally used in which the orientation of the kernel is ignored and only the individual scaling factors for each of the axes are taken into account (i.e. the diagonal matrix of *H*). If all variables are similarly distributed (except for a scaling factor), then a further simplification can be made by assuming the same bandwidth for each axis after pre-scaling the variables such that they have the same variance. Most approaches for bandwidth determination are heuristic or approximate (Scott, 1992; Wand and Jones, 1995). For low (such as two) dimensional space, there are few principled methods to estimate non-isotropic bandwidth parameters (Botve, et al., 2010). Adaptive bandwidth selection methods have also been proposed using MCMC techniques (Zhang et al., 2006).

BAYESIAN DECODING. To infer the uncertainty or probability of a hidden stimulus $\boldsymbol{x}_t$ at time *t* given the observed *m* spike events with associated features $\boldsymbol{a}_{1:m}$, we resort to Bayes' rule:

$$P(\boldsymbol{x}_t|\boldsymbol{a}_{1:m}) = \frac{P(\boldsymbol{a}_{1:m}|\boldsymbol{x}_t)P(\boldsymbol{x}_t)}{P(\boldsymbol{a}_{1:m})} \tag{11}$$

Bayes' rule provides a way to combine prior information about the stimulus $P(\boldsymbol{x}_t)$ with information obtained from observations through the likelihood function $P(\boldsymbol{a}_{1:m}|\boldsymbol{x}_t)$ (taken from Eqs. 2 and 3). The denominator $P(\boldsymbol{a}_{1:m})$ is a normalizing constant such that the posterior $P(\boldsymbol{x}_t|\boldsymbol{a}_{1:m})$ is a proper probability distribution. The posterior distribution contains all information about the stimulus at time *t* that can be extracted from the observed spike events. If a non-informative temporal prior is assumed, then the aim of Bayesian decoding is to maximize the product of the likelihood and time-independent prior: $P(\boldsymbol{x}|\boldsymbol{a}_{1:m}) \propto P(\boldsymbol{a}_{1:m}|\boldsymbol{x})P(\boldsymbol{x})$. If a completely non-informative prior is assumed, then Bayesian decoding is analogous to maximum likelihood estimation: $P(\boldsymbol{x}|\boldsymbol{a}_{1:m}) \propto P(\boldsymbol{a}_{1:m}|\boldsymbol{x})$.

IMPLEMENTATION. The spike feature based decoder was implemented in Matlab (The Mathworks, Natick, MA) with custom C extensions. In Eqs. 6-10 we developed a representation for the rate functions $\lambda(\boldsymbol{a}, \boldsymbol{x})$ and $\lambda(\boldsymbol{x})$, which are needed to compute the likelihood in Eq. 2. The rate functions can either be pre-computed at a user defined grid to construct look-up tables, or they can be evaluated online during decoding. Pre-computing the rate functions has the advantage that the computational load for decoding is low, making it suitable for real time applications. When densities need to be evaluated at a fine grid for high-dimensional feature vectors and/or stimulus vectors, then the pre-computing approach becomes impractical. In that case, the rate functions may be evaluated at a coarser grid, at the expense of decoding accuracy. Instead, here we chose to evaluate the rate function $\lambda(\boldsymbol{a}, \boldsymbol{x})$ on the fly during decoding at a user-defined grid in stimulus space. $\lambda(\boldsymbol{x})$ was pre-computed at the same stimulus grid. A small offset (0.1 Hz) was applied to both rate functions to avoid cases in which the rate is zero at all nodes in the stimulus grid (Zhang et al., 1998; Davidson et al., 2009). Decoding is performed separately for pre-defined time bins. For each detected spike and its associated features within a time bin, the rate function $\lambda(\boldsymbol{a}, \boldsymbol{x})$ (Eq. 6) is evaluated, after which the likelihood (Eqs. 2 and 3) and the posterior distributions (Eq. 11) are computed. Computations are performed in log-space, such that products in Eq. 2 are replaced by summations.

Application to hippocampal recordings

ELECTROPHYSIOLOGY AND BEHAVIOR. Eight male Long-Evans rats, weighing between 400 and 600 grams, were implanted with custom-made micro-drive arrays (Kloosterman et al., 2009; Nguyen et al., 2009). Individual arrays carried between 9-24 independently moveable tetrodes targeted to either the right dorsal hippocampus or bilaterally to both hippocampi (coordinates:

2.5 mm lateral and 4.0 mm posterior to bregma). The tetrodes were slowly lowered into the brain until they reached the cell layer of CA1 two to four weeks following array implantation. A reference electrode was positioned in the white matter overlying the dorsal hippocampus. In the case of bilateral recordings, separate ipsilateral references were used for each hippocampus. Signals were filtered between 300 Hz - 6 kHz and all extracellular spike waveforms that crossed a preset amplitude threshold (73uV) on any of the four tetrode channels were sampled at 31250 Hz (32 samples per spike waveform) and saved to disk.

During 30-60 minute long recording sessions rats were allowed to freely explore a ~3 m long linear or circular track. While no behavioral restrictions were placed on the rats, they did receive a small food reward (chocolate sprinkle, fruit loop, etc.) to encourage exploration. The position of the rats was tracked at 30 Hz using an overhead video camera and infrared light emitting diodes mounted on the implanted micro-drive array. All experiments were conducted under the supervision of the Massachusetts Institute of Technology Committee on Animal Care and followed the guidelines of the US National Institute of Health.

DECODING OF ANIMAL'S POSITION. Data collected in a recording session was divided into a training set for construction of the encoding model, and a testing set for evaluation of the decoding. In both data sets only RUN epochs, when the animals were actively moving along the track at a speed higher than 10 cm/s, were selected for further analyses. The stimulus of interest $\boldsymbol{x}$ corresponds to the one-dimensional position of the animals along the track. Only spikes of putative pyramidal cells (spike peak-trough latency > 0.35 ms) with a minimum peak amplitude of 75 μV were selected for decoding analysis. A four dimensional spike feature vector $\boldsymbol{a}$ was constructed from the spike waveform peak amplitudes on each tetrode. To establish a kernel

density based estimate of the rate functions we used a truncated Gaussian kernel (cut-off at 2 standard deviations) for both the spike amplitude dimensions and the position dimension. For spike amplitude an isotropic kernel was used with the same kernel bandwidth in all four dimensions. The rate functions were evaluated at a regular grid with 2 cm intervals that spanned the whole track. For decoding, the testing data set was divided into non-overlapping 250 ms long time bins and spikes within each bin were used to compute the posterior distribution of position according to Eq. 11.

In the Bayesian decoding framework, the decoding performance is determined both by the choice of encoding model and prior knowledge of the stimulus. Here we focus on the contribution of the novel formulation of the encoding model that includes spike waveform features and hence we chose to use a non-informative prior, making the decoding similar to maximum likelihood estimation.

The decoding error in each time bin was computed as the shortest distance along the track between the true (observed) position at the center of the time bin and the *maximum a posteriori* (MAP) estimate of position. To assess decoding performance, we analyzed the cumulative distribution of decoding error, the median error and the confusion matrix.

SPIKE SORTING BASED DECODING. Spikes of putative pyramidal neurons (spike peak-trough latency > 0.35 ms, minimum peak amplitude > 75 μV) in RUN epochs were selected prior to sorting. Spikes were automatically sorted with KlustaKwik (version 2.0.1; http://klustakwik.sourceforge.net/; see (Harris et al., 2000)) using three features per electrode: spike waveform energy and the first two principal components (PCs) of the energy-normalized spike waveform. For each cluster a set of four quality metrics was computed: L_{ratio} and isolation

distance ("IsoD"; using waveform energy and 1st PC for each channel; see (Schmitzer-Torbert et al., 2005)), fraction of inter-spike intervals smaller than 2 ms ("ISI") and the mahalanobis distance of the cluster to the spike amplitude threshold ("Dthreshold"; using spike amplitudes on the electrode with largest mean spike amplitude). Only clusters that met the following criteria were retained: $L_{ratio}<0.1$, IsoD>20, ISI<2% and $D_{threshold}>1$. The remaining clusters were collapsed into a single noise or "hash" cluster. The spatial tuning curve of each cluster was constructed using kernel-density estimation with a truncated Gaussian kernel with an optimized spatial bandwidth and the likelihood was computed according to Eq. 4.

BANDWIDTH SELECTION. We used a diagonal bandwidth matrix to compute the kernel density estimates in Eqs. 8-10. Since the spike features that were used for decoding all represent the same physical quantity (i.e. spike peak amplitude) with a similar distribution, the same scalar bandwidth (h_a) was selected for all the feature dimensions and for all tetrodes. A separate bandwidth (h_x) was chosen for the stimulus dimensions (i.e. position on track). For each separate dataset, optimal values for h_a and h_x were determined by a 2-fold cross-validation procedure on the training set.

RESULTS

A total of 12 datasets from 8 rats were used to test the spike feature based decoding approach. Table 1 summarizes the experimental data and Table 2 tabulates the decoding results, as discussed in more detail below.

Figure 2A-C shows an example of decoding the position of a rat (dataset SL14, see Table 1) using the peak amplitudes of recorded hippocampal spikes as feature vector. Qualitatively, our estimates of the rat's position on the track accurately follow its true position during periods of locomotion (Fig. 2A). To assess the decoding performance, we computed a confusion matrix (Fig. 2B) and the distribution of errors (Fig. 2C). In this example, the median decoding error is 3.6 cm and 90% of the errors fall within 10.3 cm. The confusion matrix shows a dominant diagonal structure, which indicates a high accuracy of decoding at most locations along the track. At the population level, the median decoding error across all datasets varied from 3.2 cm to 6.2 cm, with an average median error of 4.9 cm (see Table 2, column 2).

In principle, the decoder has access to information conveyed by both the population firing rate and the specific spike amplitude vectors. To investigate the extent to which spike amplitude information aids in the decoding of position in the spike feature decoding approach, we compared the performance to a decoder based on spike timing alone using a single spatial tuning curve for each tetrode (multi-unit activity (MUA) decoder; see (Fraser et al., 2009)). In all datasets the error distribution of the MUA decoder is significantly worse than the error distribution of the spike feature decoder (one-sided two-sample Kolmogorov-Smirnov test, $p <$

294 10^{-5} for all datasets; see example in Fig. 2C). Overall, the median error was significantly reduced
295 when spike amplitude information was included in our spike feature based decoding approach
296 (Fig. 2D; paired rank-sum test, $p = 4.9\times10^{-4}$).
297 Next, we examined the dependence of decoding performance on the number of spike waveform
298 features included in the analysis. Spike amplitudes on one or two electrodes of each tetrode were
299 selected as features for decoding. Since the spike amplitude threshold was applied after electrode
300 selection, fewer spikes were included in these datasets (Table 4). For both the one amplitude
301 feature and two amplitude feature case, decoding performance was higher than the corresponding
302 MUA decoder (not shown). Increasing the number of amplitude features from one to two or from
303 two to four, significantly lowered the median decoding error (paired rank-sum test: $p = 9.8\times10^{-4}$),
304 with relative mean benefits of 26% and 14% respectively.
305 The decoding performance is critically dependent on the choice of kernel bandwidths h_a and h_x.
306 Optimal bandwidths that minimized decoding error were selected separately for each decoder
307 variant and each dataset (Table 3; see Methods). For the spike feature decoder bandwidths
308 clustered around $h_x = 6$ cm and $h_a = 24$ μV (Fig. 3). Decoding performance decreased gradually
309 for increasing bandwidths. If the bandwidths were fixed at $h_x = 6$ cm and $h_a = 24$ μV for all
310 datasets, the mean deviation from the median error obtained when optimized bandwidths were
311 used was 5% (maximum: 17%). This suggest that even in cases where cross-validation is
312 impractical, appropriate fixed bandwidth parameters selected a priori may still yield near optimal
313 decoding performance for distinct datasets.
314
315 *Comparison with decoding using sorted single-units*
316 Next, we compared the spike feature decoding approach to the standard practice in which spikes

317 recorded on tetrodes are first sorted into separate single units ("cluster tag decoder", see (Zhang
318 et al., 1998)). The automated sorting procedure produced a large number of putative clusters, of
319 which 9-56 clusters across all datasets met the minimum quality criteria (Table 1), and the
320 fraction of sorted spikes out of all putative pyramidal neuron spikes ranged from 6% to 21%. The
321 remaining clusters on each tetrode were grouped into a separate hash cluster that was also
322 included in the decoding. At the group level, the spike feature decoder resulted in a significantly
323 lower median error than the cluster tag decoder (Fig. 4A; paired rank-sum test, $p = 0.0068$) with
324 an average improvement of 14%.
325 We next applied the spike feature decoding approach separately to spikes in the well-isolated
326 clusters and spikes in the hash, and compared the performance to the equivalent cluster tag
327 decoder (Fig. 4B). For both decoders, the performance significantly decreased when only the
328 well-isolated clusters or only the hash clusters were used (paired rank-sum test; spike feature
329 decoder: clusters+hash vs. clusters only $p = 4.9\times10^{-4}$, clusters+hash vs. hash only $p = 4.9\times10^{-4}$;
330 cluster tag decoder: clusters+hash vs. clusters only $p = 0.0024$, clusters+hash vs. hash only $p =$
331 4.9×10^{-4}). When only the well-isolated clusters were used for decoding, the spike feature decoder
332 showed a tendency towards a lower median error (average benefit: 7%; paired rank-sum test: $p =$
333 0.043). In contrast, the spike feature decoder performed significantly better than the cluster tag
334 decoder when only the hash was used (average benefit: 64%; paired rank-sum test: $p = 4.9\times10^{-4}$).
335 This suggests that the improved performance of the spike feature decoder is mainly due to the
336 extraction of more information from the hash.
337 For the purpose of decoding, clusters of sorted spikes do not need to correspond to single units
338 (Ventura, 2008). The cluster tag decoder may therefore benefit from using the original sorted
339 spike clusters output by KlustaKwik, regardless of their quality and without grouping poorly

isolated or multi-unit clusters into a hash cluster. Indeed, in this case the cluster tag decoder and the spike feature decoder showed comparable performance (paired rank-sum test: $p = 0.8984$). Spike sorting quality depends on the number of (informative) spike waveform features. With fewer features, cluster isolation becomes poorer and hence decoding performance in the cluster tag decoder will decrease. The spike feature decoder taps into the same information in the spike waveform features as spike sorting, and we showed previously that decoding performance decreases when fewer features are available (Fig. 2E). Here we investigated the relative performance of the spike feature decoder versus the cluster tag decoder when fewer features from a single electrode are available. Spike sorting proceeded as for tetrodes and resulted in fewer well-isolated clusters (Table 4). In this scenario, the spike feature decoder significantly outperformed the cluster tag decoder (Fig. 4D; paired rank-sum test $p = 0.0068$), with an average improvement that is higher than the four-amplitude tetrode scenario (38% vs. 14%). This result suggest that the relative benefit of using the spike feature decoder may be higher when fewer spike features are available for spike sorting.

Online encoding-decoding paradigm

Both encoding and decoding phases of the spike feature decoding paradigm can be performed with minimal supervision, provided that suitable bandwidth parameters have been selected. As such, this new paradigm is well suited for online encoding and decoding of stimuli from ongoing neural activity as is required for brain-computer interfaces. As a demonstration we simulate an experiment in which the position of a rat is estimated as it explores a novel linear track for the first time. As soon as the rat enters the new environment, neural data is acquired and for every 250 ms time bin in which the rat is actively moving (speed > 10 cm/s) the recorded spikes and

their waveform features are used to compute an estimate of position. Subsequently, the encoding model is updated using the newly acquired spikes, their waveform features and the rat's physical location in the track. Thus at any given time decoding is performed using only the recorded spike data in the past. Figure 5A shows the position estimates for the first two laps and the last lap on the track for one dataset (SL14). The estimates in the first lap of behavior are biased towards past positions as this is the only information available in the spiking. However, in subsequent laps the decoding error decreases and quickly reaches an asymptotic value (Fig. 5B). These results suggest that only a limited amount of spiking history may be necessary to achieve accurate decoding results when online real time encoding and decoding is required.

DISCUSSION

We have demonstrated a novel Bayesian neural decoding approach that implements a direct mapping between spike waveform features and a sensory stimulus or other covariates. This new approach has several important advantages over other methods. First, the spike feature decoder uses both the timing and waveform features of all available spike events to increase the amount of stimulus-related information that can be extracted from the neural signals. Second, there is no need for an intermediate spike-sorting step that adds complexity and may lead to loss of information. Third, our approach defines a non-parametric encoding model to flexibly describe the relation between the stimulus and neural activity. And finally, the spike feature decoder allows both encoding and decoding stages to be performed with minimal supervision.

We tested the new decoding method on tetrode recordings from the hippocampus in freely behaving rats and showed that the animal's location on a track could be accurately estimated. In our tests we used spike peak amplitude as the feature for decoding, however it is possible to use any other set of spike features as well, for example waveform width, wave-shape parameters, or principal components. Our approach takes advantage of the same spike waveform information as most spike sorting methods, but does so without an explicit sorting step. Our results show a small benefit of the spike feature decoder compared to a standard cluster tag decoder, as the new approach extracts more information from the poorly separable hash spikes.

It is noteworthy to point out the key differences between our approach and other paradigms in which neural spiking data was used for decoding without a spike sorting step. Fraser et al. (2009)

fitted multi-unit activity responses to movement with a spline function and thus each electrode was treated as a single "virtual" unit. This approach may work well if only a few neurons are recorded on each electrode, or if all neurons contributing to the multi-unit activity have similar tuning properties. However, this method will likely perform poorly if the MUA contains spikes from many neurons with diverse responses, for example in the hippocampus as we showed here. Stark and Abeles (2007) presented another interesting approach in which multi-unit activity, defined as the root-mean-square of the 300 Hz – 6 kHz band of the local field potential, was used to predict arm movement in monkeys. In this method, spiking activity was not modeled explicitly and decoding was performed by a support vector machine classifier. Unlike our approach, the measure of multi-unit activity in Stark and Abeles (2007) does not separate the contributions of spike rate and amplitude, nor does it allow incorporation of other waveform features.

Ventura (2008) proposed a paradigm in which the identities of neurons are extracted implicitly from the spike train recorded on a single electrode by assuming a known parametric model for the neurons' tuning to the stimulus. This approach worked well in simulations, but was not applied to real data set and it is not clear if the method will work equally well for populations of neurons with complex, non-parametric tuning functions. In addition, the decoding step assumes that the temporal evolution of the stimulus is smooth (Ventura, 2008). This assumption is not necessarily true or known to be true, for example if the goal is to decode a hidden stimulus with unknown temporal dynamics (Davidson et al., 2009; Kloosterman, 2011).

More recently, Ventura proposed to exploit the information in covariates that modulate neuronal firing ("tuning information") in addition to spike waveform information to improve spike sorting (Ventura, 2009a) with application in decoding as well (Ventura, 2009b). Ventura's approach uses a similar mapping between waveform features and covariates as we have done in

the spike feature decoder, however, parametric models are used rather than the non-parametric approach in our work.

Luczak and Narayanan (2005) avoided spike sorting by constructing a “spectral representation” of the neural data by considering a discrete space of spike waveform features (they used principal components) and time. The spectral representation of Luczak and Narayanan is similar to the spike feature-marked point process that is at the basis of our method. Using a combination of partial least squares to select stimulus-relevant features and linear discriminant analysis for classification, they demonstrated that the spectral representation can be used to successfully discriminate between two discrete auditory stimuli. In contrast, we used a naive Bayesian approach in which spiking statistics are explicitly modeled, and which we applied to the decoding of a continuously time-varying stimulus.

The main strength of the proposed spike feature decoding approach is that it provides straightforward stimulus estimation from information-rich spiking data in a minimally supervised manner. The method can be applied in online and real time encoding/decoding scenarios, which makes it appealing for brain machine interfaces and neural prosthetics that use chronic implants. By utilizing the information carried by all spikes, whether or not they can be uniquely assigned to a single neuron, the spike feature decoding approach is more robust to changes in signal quality as observed in chronic recording applications. In addition, non-stationarity of the neural signals which is commonly encountered in long-term recordings and slow changes in the encoding model can be easily handled by restricting the spike events that contribute to the encoding model to a finite temporal window.

The spike feature decoding approach is not fully unsupervised as it requires the selection of

443 appropriate kernel bandwidth parameters. In the current experimental data analysis, a cross-
444 validation approach was employed to estimate the two bandwidth parameters for spike
445 amplitude and position dimensions. We found that the decoding performance was
446 relatively robust around suboptimal bandwidth parameters, suggesting that a prior
447 selection of a fixed bandwidth may be appropriate.
448
449 For online applications it is important that the computations for encoding and decoding stages
450 can be performed in real time. In our current implementation encoding is cheap (all recorded
451 spikes are simply retained), whereas decoding is computationally intensive. The complexity of
452 decoding scales with the total number of spike events incorporated in the encoding model.
453 Several strategies can be used to decrease the computational burden. If pre-computation of the
454 rate function is practical, then this would avoid costly evaluation of the densities during
455 decoding. If necessary, a trade-off can be made between decoding performance and computation
456 speed by reducing the number of dimensions of the feature space. For example, using two
457 amplitude features (from a stereotrode) instead of four features (from a tetrode) gives acceptable
458 (albeit decreased) decoding performance. Alternatively, it is possible to reduce computational
459 load of online density evaluation by exclude groups of low-informative spike events based on
460 their waveform properties. For example, in the hippocampus most stimulus-relevant information
461 is carried by pyramidal neuron activity and therefore in our tests we filtered out spikes from
462 putative interneurons (peak-trough latency < 0.35 ms). This selection of spikes substantially
463 reduced the computational burden without significantly affecting decoding performance. A
464 further reduction can be achieved by increasing the spike amplitude threshold, excluding low
465 amplitude spikes that carry relatively little information. Another way to alleviate this problem, is

466 to find compact and efficient representations of the kernel density estimates of the rate functions
467 (Mitra et al., 2002; Girolami, 2003; Zhou et al., 2003; Huang and Chow, 2006).
468
469 Our decoding algorithm is based on the statistical assumption that the spike events follow a
470 spatio-temporal Poisson process (i.e. spike events are mutually independent in both spike feature
471 space and time). This is equivalent to assuming an independent Poisson rate code for all neurons
472 in the ensemble. In our example, the encoding model is constructed from multiple presentations
473 of the same stimulus, and even if individual spike trains do not follow a Poisson distribution, the
474 aggregate of many such spike trains will. Although the Poisson assumption is over-simplified for
475 most experimental data, it provides us with a simple and tractable solution for decoding analysis.
476 It is possible to relax the assumptions of Poisson statistics and independence - for example to
477 incorporate temporal dependence the spike history in each electrode can be represented as an
478 augmented temporal feature. Alternatively, the spatial local dependence can be modeled by
479 considering a Neyman-Scott process (Diggle, 2003) or a Poisson cluster process (Bartlett, 1964;
480 Wolpert and Ickstadt, 1998). These topics will be the subject of future investigations.
481
482 Our decoding paradigm can be extended in several ways. For instance, we can reformulate the
483 Bayesian decoding problem within the state-space framework by inclusion of a smooth temporal
484 prior (Brown et al., 1998). A temporal prior can be useful for reconstruction of stimuli or
485 covariates that are known to smoothly change over time, such as the position of rat or the
486 movement of an arm. The spike feature decoding can also be used to extract information from
487 ensemble spiking activity by estimating the mutual information and entropy of the stimulus and
488 neural responses. Estimation of these information measures may provide a better understanding

489 the underlying principles of neural codes used in the brain (Jacobs et al., 2009; Quian Quiroga
490 and Panzeri, 2009).
491

ACKNOWLEDGMENTS

We thank Greg Hale and Jun Yamamoto for contributing their datasets. This work was supported by the NIH Grant MH061976 and ONR MURI N00014-10-1-0936 grant to M. A. Wilson. Z. Chen was supported by an Early Career Award from the Mathematical Biosciences Institute (MBI) and the NSF-CRCNS (Collaborative Research in Computational Neuroscience) grant.

499 REFERENCES

500 **Bartlett MS**. The spectral analysis of two-dimensional point processes. *Biometrika* 51: 299–311,
501 1964.

502 **Boloori A-R, Jenks RA, Desbordes G, Stanley GB**. Encoding and decoding cortical
503 representations of tactile features in the vibrissa system. *J Neurosci* 30: 9990–10005, 2010.

504 **Botev ZI, Grotowski JF, Kroese DP.** Kernel density estimation via diffusion. Ann. Stat. 38:
505 2916-2957, 2010

506 **Brown EN, Frank LM, Tang D, Quirk MC, Wilson MA**. A statistical paradigm for neural
507 spike train decoding applied to position prediction from ensemble firing patterns of rat
508 hippocampal place cells. *J Neurosci* 18: 7411–25, 1998.

509 **Chapin JK**. Using multi-neuron population recordings for neural prosthetics. *Nat Neurosci* 7:
510 452–5, 2004.

511 **Davidson TJ, Kloosterman F, Wilson MA**. Hippocampal replay of extended experience.
512 *Neuron* 63: 497–507, 2009.

513 **Diggle PJ**. *Statistical Analysis of Spatial Point Patterns*. 2nd ed. Oxford University Press, 2003.

514 **Fraser GW, Chase SM, Whitford A, Schwartz AB**. Control of a brain-computer interface
515 without spike sorting. *J Neural Eng* 6: 055004, 2009.

516 **Georgopoulos a P, Schwartz a B, Kettner RE**. Neuronal population coding of movement
517 direction. *Science* 233: 1416–9, 1986

518 **Girolami M**. Probability density estimation from optimally condensed data samples. *IEEE*
519 *Transactions on Pattern Analysis and Machine Intelligence* 25: 1253–1264, 2003.

520 **Goodman IN, Johnson DH**. Information theoretic bounds on neural prosthesis effectiveness:
521 The importance of spike sorting. In: *2008 IEEE International Conference on Acoustics, Speech*
522 *and Signal Processing*. IEEE, p. 5204–5207.

523 **Gupta AS, Van der Meer M a a, Touretzky DS, Redish a D**. Hippocampal replay is not a
524 simple function of experience. *Neuron* 65: 695–705, 2010.

525 **Harris KD, Henze DA, Csicsvari J, Hirase H, Buzsáki G**. Accuracy of tetrode spike
526 separation as determined by simultaneous intracellular and extracellular measurements. *Journal*
527 *of neurophysiology* 84: 401–14, 2000.

Hochberg LR, Bacher D, Jarosiewicz B, Masse NY, Simeral JD, Vogel J, Haddadin S, Liu J, Cash SS, Van der Smagt P, Donoghue JP. Reach and grasp by people with tetraplegia using a neurally controlled robotic arm. *Nature* 485: 372–5, 2012.

Huang D, Chow TWS. Enhancing density-based data reduction using entropy. *Neural Comput* 18: 470–95, 2006.

Huys QJM, Zemel RS, Natarajan R, Dayan P. Fast population coding. *Neural Comput* 19: 404–41, 2007.

Jacobs AL, Fridman G, Douglas RM, Alam NM, Latham PE, Prusky GT, Nirenberg S. Ruling out and ruling in neural codes. *Proc Natl Acad Sci U S A* 106: 5936–41, 2009.

Kloosterman F, Davidson TJ, Gomperts SN, Layton SP, Hale G, Nguyen DP, Wilson MA. Micro-drive array for chronic in vivo recording: drive fabrication. *J Vis Exp* , 2009.

Kloosterman F. Analysis of Hippocampal Memory Replay Using Neural Population Decoding. *Neuronal network analysis: concepts and experimental approaches. (Neuromethods)* : 259–282, 2011.

Luczak A, Narayanan NS. Spectral representation--analyzing single-unit activity in extracellularly recorded neuronal data without spike sorting. *J Neurosci Methods* 144: 53–61, 2005.

Mitra P, Murthy C, Pal S. Density-based multiscale data condensation. *Pattern Analysis and Machine ...* 24: 734–747, 2002.

Nguyen DP, Layton SP, Hale G, Gomperts SN, Davidson TJ, Kloosterman F, Wilson MA. Micro-drive array for chronic in vivo recording: tetrode assembly. *J Vis Exp* , 2009.

Paninski L, Pillow J, Lewi J. Statistical models for neural encoding, decoding, and optimal stimulus design. *Prog Brain Res* 165: 493–507, 2007.

Quian Quiroga R, Panzeri S. Extracting information from neuronal populations: information theory and decoding approaches. *Nat Rev Neurosci* 10: 173–85, 2009.

Sanger T. Neural population codes. *Current Opinion in Neurobiology* 13: 238–249, 2003.

Schmitzer-Torbert N, Jackson J, Henze D, Harris K, Redish AD. Quantitative measures of cluster quality for use in extracellular recordings. *Neuroscience* 131: 1–11, 2005.

Schwartz AB, Cui XT, Weber DJ, Moran DW. Brain-controlled interfaces: movement restoration with neural prosthetics. *Neuron* 52: 205–20, 2006.

Scott DW Multivariate Density Estimation: Theory, Practice, and Visualization. John Wiley & Sons, New York, 1992.

560 **Stark E, Abeles M**. Predicting movement from multiunit activity. *J Neurosci* 27: 8387–94,
561 2007.

562 **Truccolo W, Eden UT, Fellows MR, Donoghue JP, Brown EN**. A point process framework
563 for relating neural spiking activity to spiking history, neural ensemble, and extrinsic covariate
564 effects. *Journal of neurophysiology* 93: 1074–89, 2005.

565 **Ventura V**. Spike train decoding without spike sorting. *Neural Comput* 20: 923–63, 2008.

566 **Ventura V**. Automatic spike sorting using tuning information. *Neural Comput* 21: 2466–501,
567 2009a.

568 **Ventura V**. Traditional waveform based spike sorting yields biased rate code estimates. *Proc*
569 *Natl Acad Sci U S A* 106: 6921–6, 2009b.

570 **Wand MP, Jones MC.** Kernel Smoothing. Chapman & Hall/CRC, London, 1995.

571 **Wolpert R, Ickstadt K**. Poisson/gamma random field models for spatial statistics. *Biometrika*
572 85: 251–267, 1998.

573 **Wood F, Black MJ**. A nonparametric Bayesian alternative to spike sorting. *J Neurosci Methods*
574 173: 1–12, 2008.

575 **Zhang K, Ginzburg I, McNaughton BL, Sejnowski TJ**. Interpreting neuronal population
576 activity by reconstruction: unified framework with application to hippocampal place cells.
577 *Journal of neurophysiology* 79: 1017–44, 1998.

578 **Zhou A, Cai Z, Wei L, Qian W**. M-kernel merging: towards density estimation over data
579 streams. In: *Eighth International Conference on Database Systems for Advanced Applications,*
580 *2003. (DASFAA 2003). Proceedings.* IEEE, p. 285–292.

581 **Zhang X, King ML, Hyndman RJ.** A Bayesian approach to bandwidth selection for
582 multivariate density estimation. J. Computational Statistics & Data Analysis, 50: 3009-3031,
583 2006.

584 **Zhuang J, Truccolo W, Vargas-Irwin C, Donoghue JP**. Decoding 3-d reach and grasp
585 kinematics from high-frequency local field potentials in primate primary motor cortex. *IEEE*
586 *Trans Biomed Eng* 57: 1774–84, 2010.

587
588
589

Table 1. Summary of experimental data (datasets ranked by # clusters)

Dataset	# Tetrodes	# Total Spikes	# Sorted Spikes	% Sorted Spikes	# Clusters
R1D2	14	81 K	5 K	6 %	9
R2D2	18	106 K	7 K	6 %	12
FK11	9	195 K	15 K	8 %	18
R1D1	14	170 K	36 K	21 %	29
R2D1	18	206 K	36 K	17 %	32
Esm02	17	307 K	44 K	14 %	32
Sat2	18	355 K	44 K	12 %	35
SL13	17	126 K	22 K	17 %	40
SL16	16	160 K	22 K	14 %	40
Esm01	18	222 K	30 K	14 %	48
SL14	14	215 K	43 K	20 %	52
SL15	17	330 K	43 K	13 %	56

Table 2. Summary of decoding performances across all datasets (ranked by # clusters)

	spike feature decoder			MUA decoder	identity decoder			
Dataset	all spikes	spikes in isolated clusters	spikes in hash	all spikes	isolated clusters + hash	isolated clusters	hash only	all clusters
R1D2	6.0	28.0	18.5	23.0	11.0	36.3	31.3	7.5
R2D2	6.0	18.0	13.5	12.0	7.0	21.5	17.5	7.0
FK11	6.2	9.9	7.1	25.3	7.2	9.1	23.5	5.9
R1D1	4.5	7.5	7.0	13.5	5.5	8.5	24.0	4.5
R2D1	5.5	7.5	7.0	12.0	6.0	8.5	23.0	5.0
Esm02	3.6	5.0	4.1	12.2	4.5	5.8	12.6	3.0
Sat2	6.0	6.8	6.2	12.7	6.9	7.1	16.1	5.9
SL13	4.7	4.9	6.2	13.9	4.6	5.5	19.8	4.9
SL16	3.7	4.8	4.5	18.2	4.3	4.8	34.8	3.6
Esm01	6.0	6.2	6.3	9.0	5.3	5.8	9.9	5.0
SL14	3.6	4.1	4.3	13.9	4.0	4.1	26.3	3.5
SL15	3.2	3.8	4.8	63.2	4.2	3.9	102.6	3.6

596 **Table 3.** Optimal bandwidths for decoder variants in Table 2 (datasets ranked by # clusters)

	spike feature decoder						MUA decoder	identity decoder			
Dataset	all spikes		spikes in isolated clusters		spikes in hash		all spikes	isolated clusters + hash	isolated clusters	hash only	all clusters
	h_a	h_x	h_a	h_x	h_a	h_x	h_x	h_x	h_x	h_x	h_x
R1D2	20	3.75	17.5	6.25	20	7.5	5	2.5	7.5	3.75	2.5
R2D2	22.5	3.75	17.5	6.25	17.5	6.25	5	2.5	6.25	6.25	5
FK11	20	6.25	25	7.5	25	8.75	17.5	5	6.25	11.25	6.25
R1D1	17.5	6.25	20	7.5	20	6.25	2.5	5	3.75	2.5	3.75
R2D1	27.5	5	20	7.5	17.5	6.25	2.5	2.5	3.75	2.5	5
Esm02	22.5	6.25	32.5	8.75	25	5	5	3.75	5	5	5
Sat2	20	8.75	20	7.5	30	7.5	8.75	8.75	6.25	7.5	8.75
SL13	20	3.75	17.5	7.5	22.5	6.25	5	3.75	3.75	12.5	8.75
SL16	30	8.75	30	7.5	20	6.25	12.5	7.5	7.5	10	6.25
Esm01	30	7.5	45	10	27.5	7.5	5	7.5	6.25	6.25	7.5
SL14	27.5	6.25	27.5	6.25	17.5	7.5	12.5	6.25	3.75	10	5
SL15	17.5	7.5	27.5	5	17.5	7.5	17.5	2.5	3.75	11.25	3.75

Table 4. Summary of experimental data for single electrode and stereotrode simulation (datasets ranked as in Table 1)

		stereotrode	single electrode			
Dataset	# Electrodes	# Total Spikes	# Total Spikes	# Sorted Spikes	% Sorted Spikes	# Clusters
R1D2	14	55 K	36 K	3 K	8%	7
R2D2	18	77 K	53 K	1 K	3%	4
FK11	9	146 K	104 K	6 K	6%	1
R1D1	14	132 K	102 K	9 K	8%	6
R2D1	18	158 K	121 K	12 K	10%	6
Esm02	17	237 K	163 K	25 K	16%	8
Sat2	18	290 K	218 K	4 K	2%	2
SL13	17	111 K	68 K	11 K	16%	6
SL16	16	127 K	75 K	4 K	6%	3
Esm01	18	170 K	121 K	4 K	4%	6
SL14	14	180 K	110 K	10 K	9%	3
SL15	17	280 K	164 K	11 K	6%	6

FIGURE LEGENDS

Figure 1. A. Diagram of spike waveform feature decoding approach. In the encoding stage (left), a model describing the relation between spike waveform features and the stimulus of interest (for example an animal's position) is constructed. Note that no prior sorting of the recorded spikes is required. In the decoding stage (right), the encoding model is used to obtain an estimate of the stimulus from the measured spike waveform features. **B.** Pictographic overview of major steps in the algorithm of the spike feature decoding approach. From spike waveform features computed for the recorded raw spike waveforms and the known stimulus, the probability distributions $p(\boldsymbol{a}, \boldsymbol{x})$, $p(\boldsymbol{x})$ and $\pi(\boldsymbol{x})$ are derived. From these distributions, the joined rate function $\lambda(\boldsymbol{a}, \boldsymbol{x})$ and marginal rate function $\lambda(\boldsymbol{x})$ can be derived. During the decoding process, observed spike waveform features in single time bins are used to evaluate the rate functions (indirectly through evaluation of the probability distributions $p(\boldsymbol{a}, \boldsymbol{x})$, $p(\boldsymbol{x})$ and $\pi(\boldsymbol{x})$) at a user-defined stimulus grid. The evaluated rates are used to compute the posterior distribution.

Figure 2. A. Example of spike waveform feature decoding of a rat's position during two full laps on a 3 meter long track (dataset SL14). Top: rat's true position. Middle: posterior probability distributions of the decoded position along the track computed in non-overlapping 250 ms time bins. Darker shades of gray indicate higher probabilities. Bottom: decoding error. Note that decoding error is low during periods of active motion ("RUN", indicated by thick bars above plot). **B.** Confusion matrix showing the distribution of estimated positions for all positions on the track (dataset SL14). Positions are binned in 10 cm bins for improved visualization **C.** Empirical cumulative distribution function (CDF) of decoding errors for dataset SL14. Solid line: spike

624 waveform feature decoder. Dashed line: MUA decoder. Inset shows detail of the CDFs. **D.** Box
625 plots comparing the distributions of median errors across all datasets for the spike waveform
626 feature decoder and the MUA decoder. Gray lines represent data of individual datasets. **E.** Box
627 plots comparing decoding performance when one, two or four amplitude features (from one, two
628 or four electrodes in tetrode) are used in the spike feature decoder. Outliers are indicated by '+'
629 symbol.
630
631 **Figure 3**. **A.** Optimal bandwidths h_x and h_a for spike feature decoder for all datasets. The mean
632 optimal bandwidth is indicated by the '+' symbol. Dashed grid lines indicate bandwidth values
633 used for cross-validation.
634
635 **Figure 4.** Comparison of the spike feature decoder to the standard single unit decoder for three
636 different decoding strategies. In all panels, box plots compare the median error distributions for
637 the two decoders. Gray lines represent data of all individual datasets. Outliers are indicated by
638 '+' symbol. **A.** Decoding using all spikes in isolated clusters and hash. **B.** Decoding using only
639 spikes in isolated clusters, excluding hash. **C.** Decoding using only spikes in hash. **D.**
640 Comparison of spike feature decoder and cluster tag decoder using a reduced set of spike
641 waveform features from a single electrode.
642
643 **Figure 5.** Simulated minimally supervised online decoding. **A.** Posterior probability distributions
644 for 250 ms time bins in three epochs corresponding to the first two laps and the last lap on the
645 track (dataset SL14). Darker shades of gray indicate higher probabilities. Solid line is animal's
646 true trajectory. **B.** Median decoding error computed for each lap separately. The horizontal

647 dashed line shows the mean of the median decoding error statistics across all laps.

648

649

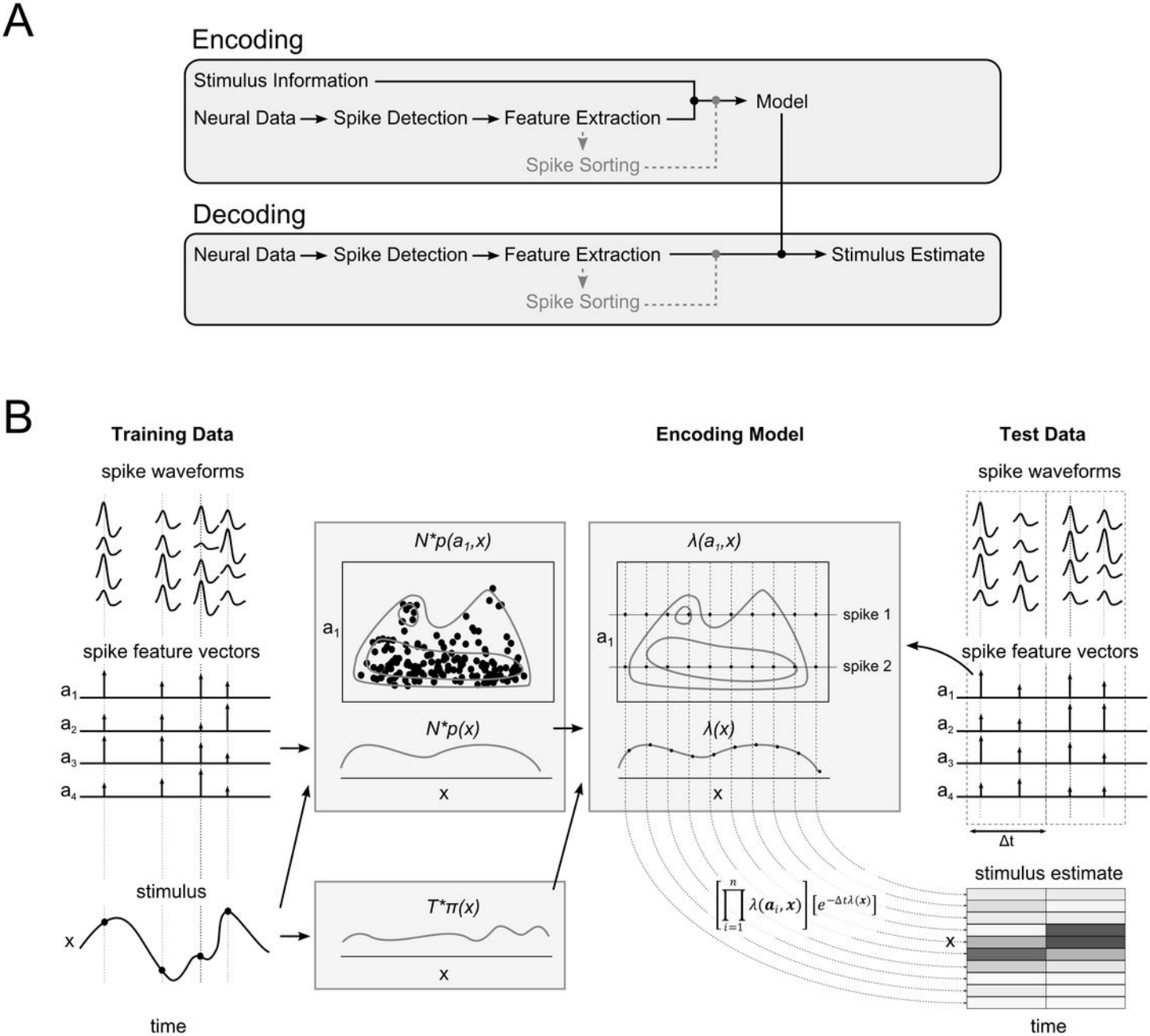
A
Encoding
Stimulus Information
Neural Data
Spike Detection
Feature Extraction
Model
Spike Sorting
Decoding
Neural Data
Spike Detection
Feature Extraction
Stimulus Estimate
Spike Sorting
B
Training Data
Encoding Model
Test Data
spike waveforms
spike feature vectors
a1
a2
a3
a4
N*p(a1,x)
N*p(x)
x
λ(a1,x)
λ(x)
spike 1
spike 2
spike waveforms
spike feature vectors
Δt
stimulus
x
time
T*π(x)
stimulus estimate
time

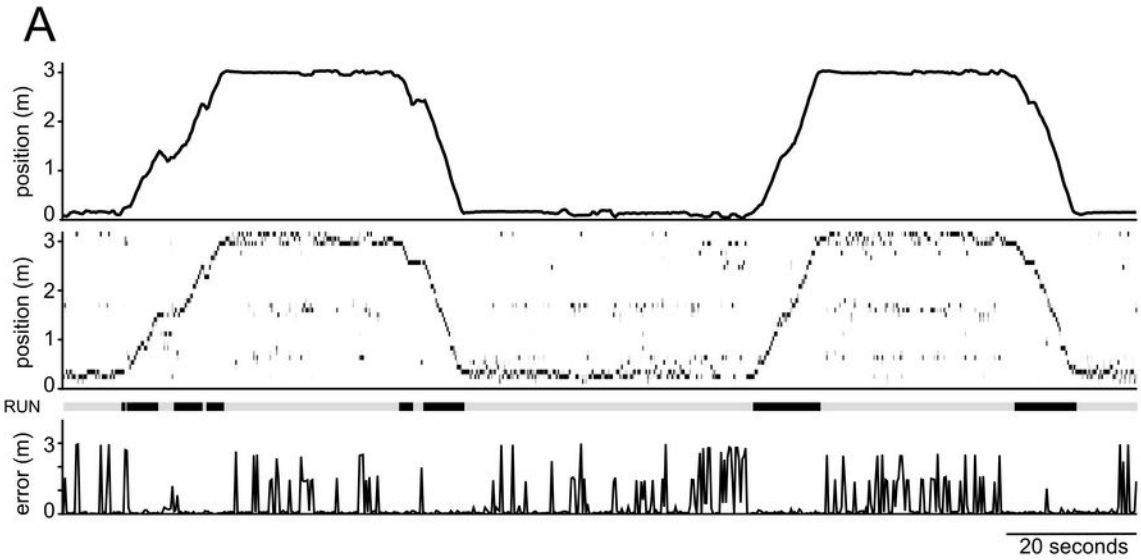
A
position (m)
position (m)
RUN
error (m)
20 seconds

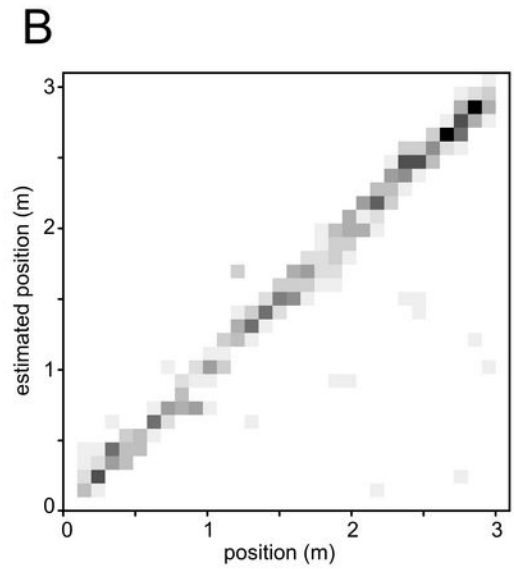
B
estimated position (m)
position (m)

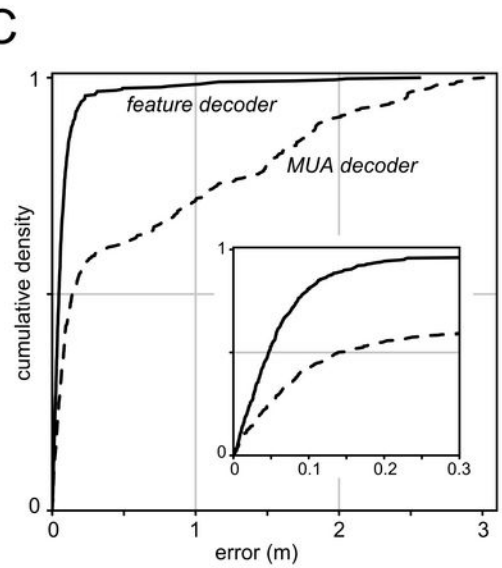
C
feature decoder
MUA decoder
cumulative density
error (m)

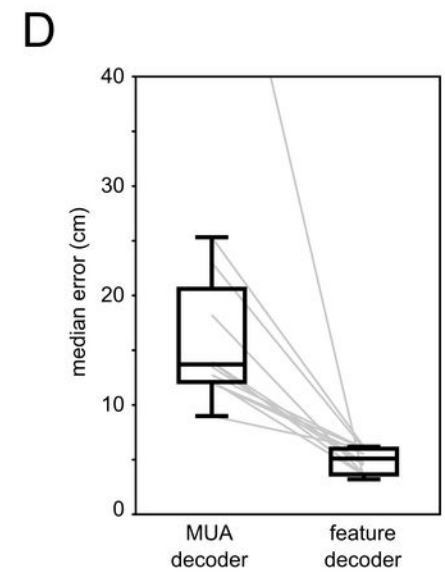
D
median error (cm)
MUA decoder
feature decoder

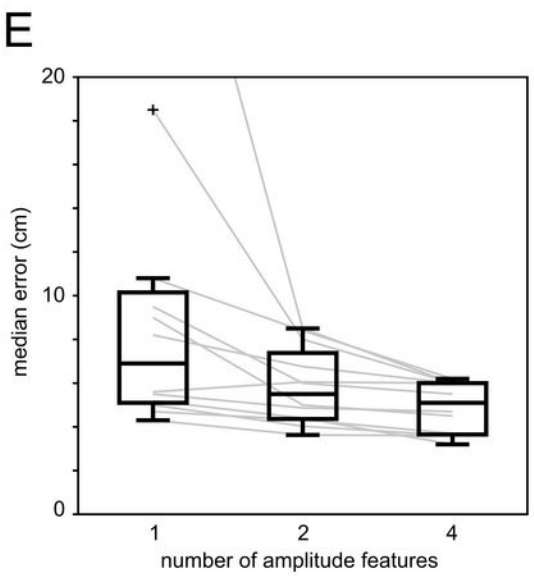
E
median error (cm)
number of amplitude features

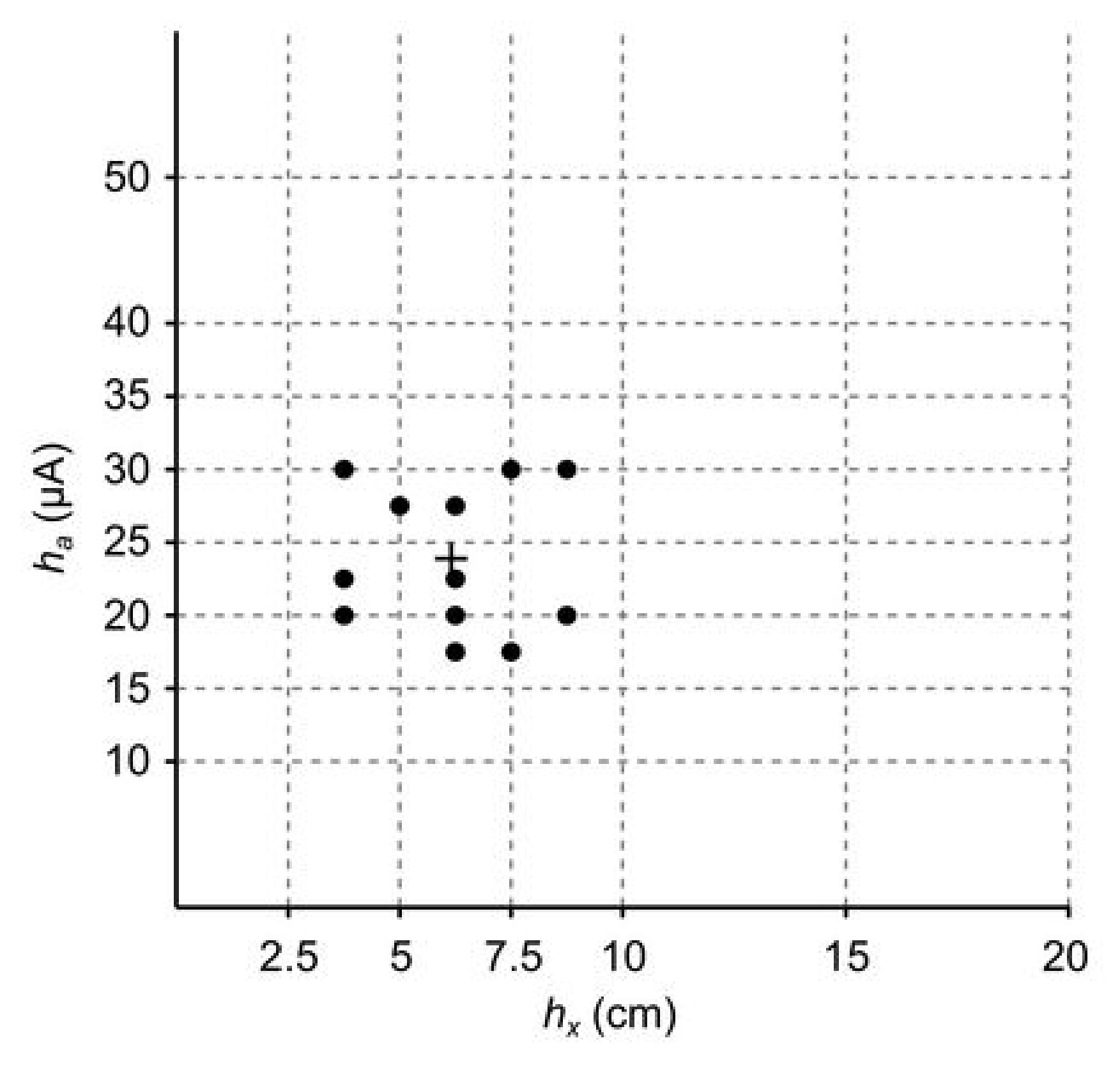
50
40
35
30
25
20
15
10
h_a (μA)
2.5
5
7.5
10
15
20
h_x (cm)

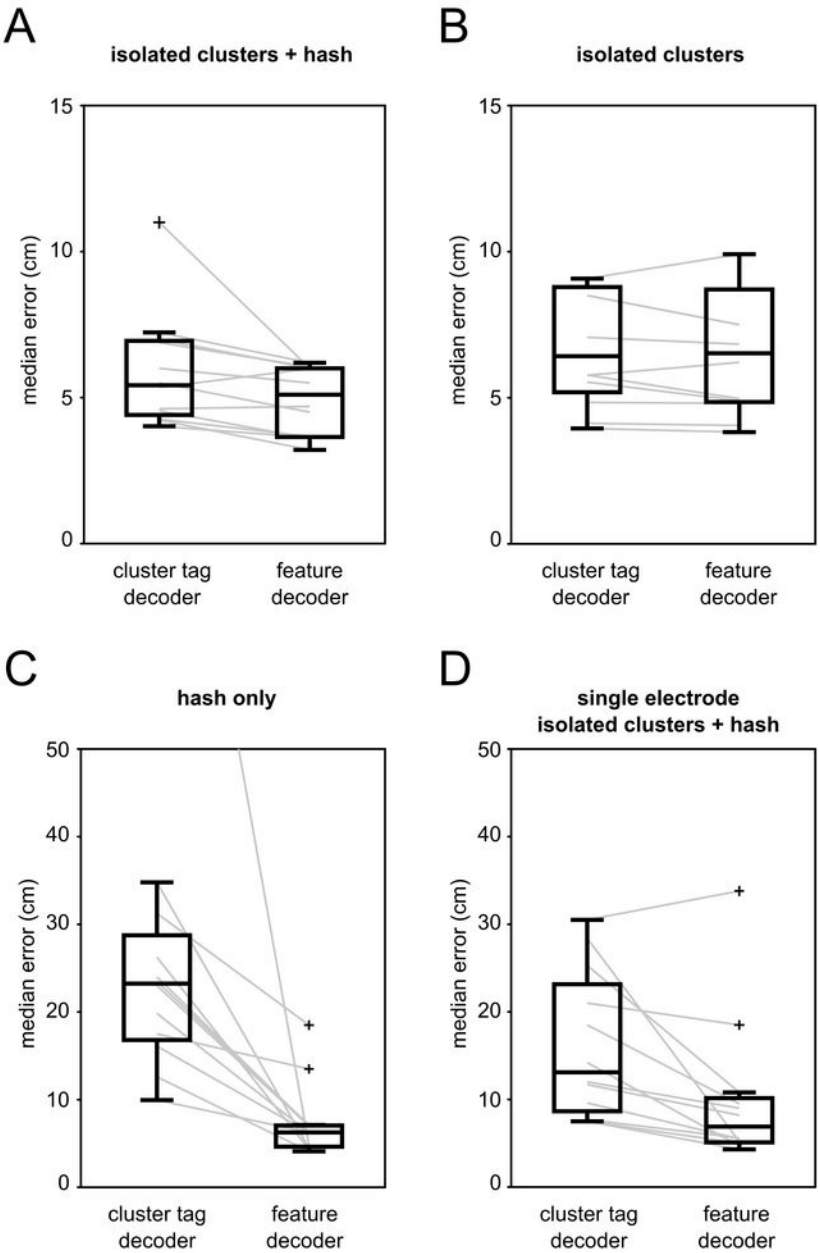
A
isolated clusters + hash
median error (cm)
15
10
5
0
cluster tag decoder
feature decoder
B
isolated clusters
median error (cm)
15
10
5
0
cluster tag decoder
feature decoder
C
hash only
median error (cm)
50
40
30
20
10
0
cluster tag decoder
feature decoder
D
single electrode isolated clusters + hash
median error (cm)
50
40
30
20
10
0
cluster tag decoder
feature decoder

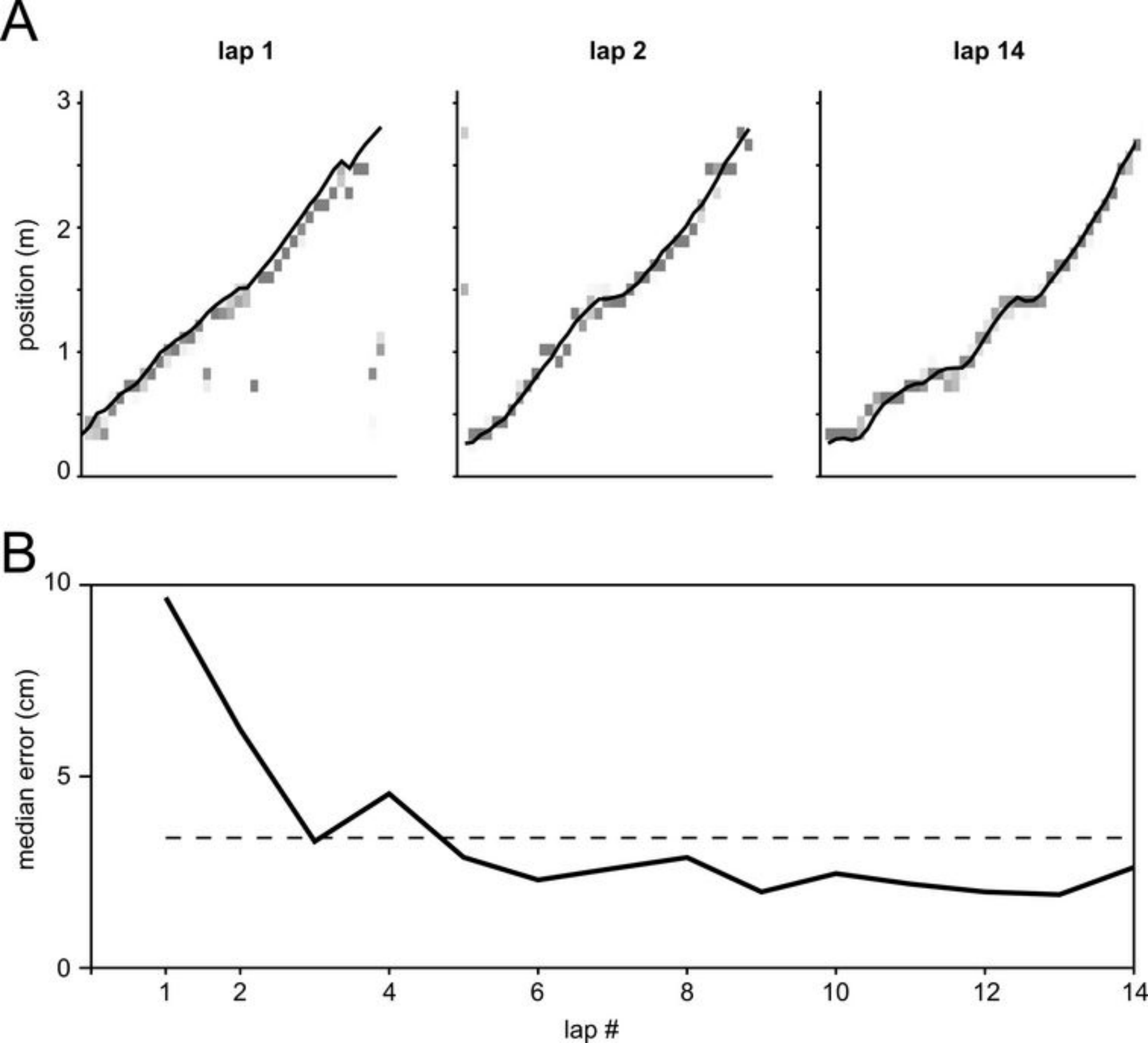
A
lap 1
lap 2
lap 14
position (m)
3
2
1
0
B
median error (cm)
10
5
0
1
2
4
6
8
10
12
14
lap #